Phosphorylation of Nanog is Essential to Regulate Bmi1 and Promote Tumorigenesis

Xiujie Xie[1,2], **Longzhu Piao**[1,2], **Greg S. Cavey**[3,4], **Matthew Old**[1,2], **Theodoros N. Teknos**[1,2], **Anna K Mapp**[5], and **Quintin Pan**[1,2]

[1]Department of Otolaryngology-Head and Neck Surgery, The Ohio State University Wexner Medical Center, Columbus, OH 43210

[2]Arthur G. James Cancer Hospital and Richard J. Solove Research Institute, The Ohio State University Comprehensive Cancer Center, Columbus, OH 43210

[3]Van Andel Research Institute, Grand Rapids, MI 49503

[4]Southwest Michigan Innovation Center, Kalamazoo, MI 49008

[5]Department of Chemistry, University of Michigan, Ann Arbor, MI 48105

Abstract

Emerging evidence indicates that Nanog is intimately involved in tumorigenesis in part through regulation of the cancer initiating cell population. However, the regulation and role of Nanog in tumorigenesis are still poorly understood. In this study, human Nanog was identified to be phosphorylated by human PKCε at multiple residues including T200 and T280. Our work indicated that phosphorylation at T200 and T280 modulates Nanog function through several regulatory mechanisms. Results with phosphorylation-insensitive and phosphorylation-mimetic mutant Nanog revealed that phosphorylation at T200 and T280 enhance Nanog protein stability. Moreover, phosphorylation-insensitive T200A and T280A mutant Nanog had a dominant-negative function to inhibit endogenous Nanog transcriptional activity. Inactivation of Nanog was due to impaired homodimerization, DNA binding, promoter occupancy, and p300, a transcriptional co-activator, recruitment resulting in a defect in target gene promoter activation. Ectopic expression of phosphorylation-insensitive T200A or T280A mutant Nanog reduced cell proliferation, colony formation, invasion, migration, and the cancer initiating cell population in head and neck squamous cell carcinoma (HNSCC) cells. The *in vivo* cancer initiating ability was severely compromised in HNSCC cells expressing phosphorylation-insensitive T200A or T280A mutant Nanog; 87.5% (14/16), 12.5% (1/8), and 0% (0/8) for control, T200A, and T280A, respectively. Nanog occupied the Bmi1 promoter to directly transactivate and regulate Bmi1. Genetic ablation and rescue experiments demonstrated that Bmi1 is a critical downstream signaling node for the pleiotropic, pro-oncogenic effects of Nanog. Taken together, our study revealed, for the first time,

Correspondence should be addressed to: Quintin Pan, The Ohio State University Wexner Medical Center, Department of Otolaryngology-Head and Neck Surgery, 442 Tzagournis Medical Research, 420 West 12th Avenue, Columbus, OH, 43210; Quintin.Pan@osumc.edu.

Conflict of Interest

The authors declare no conflict of interest.

that post-translational phosphorylation of Nanog is essential to regulate Bmi1 and promote tumorigenesis.

Keywords

Head and neck cancer; protein kinase C; p300; cancer stem cells; cancer initiating cells

Introduction

It is well recognized that Nanog, a homeodomain protein, forms a core embryonic stem cell (ESC) network with Oct4 and Sox2 to regulate ESC self-renewal and maintenance (1–5). Recent work has implicated Nanog in various epithelial malignancies, including head and neck squamous cell carcinoma (HNSCC). Nanog expression is increased in the primary tumors from HNSCC patients compared to normal adjacent epithelium (6). Moreover, elevated Nanog was reported as a prognostic biomarker for overall survival in HNSCC (7). Primary tumors from breast carcinoma patients had increased Nanog levels compared to normal breast tissue (8). Elevated Nanog was associated with high pathologic grade and poor prognosis in lung adenocarcinoma patients (9). Similarly, elevated Nanog significantly correlated with poor overall survival in colorectal carcinoma (10).

Loss-of-function studies showed that Nanog is essential in the development of breast, colorectal, and prostate carcinoma partly through regulation of the cancer initiating cell (CIC) or cancer stem cell (CSC) population (11). The Nanog-Gli1 signaling axis is indispensible to regulate glioma stem cells (12). Genetic ablation of Nanog compromised the CIC population and reduced the tumor initiating potential of HNSCC patient cells in athymic nude mice (6). Acquisition of cis-platinum resistance in OC2 HNSCC cells resulted in elevated Nanog, Oct4, and Bmi1 levels (13). Furthermore, elevated Nanog was associated with cis-platinum resistance in HNSCC patients (13). Castration-resistant prostate cancer cells possess CIC properties and have elevated levels of the core ESC transcription factors, Nanog, Oct4, and Sox2, and Bmi1 (14). Interestingly, Nanog was reported to form a heterodimer complex with Stat3 to control microRNA-21 expression and chemoresistance (15). These studies provide evidence that the role of Nanog in tumorigenesis is complex and likely involves the regulation of CICs and the bulk non-CICs as well.

The regulatory mechanisms to modulate Nanog function are still poorly understood. Post-translational modifications, including phosphorylation, often serve as a switch to dynamically regulate protein stability and function. PKCε was reported to mediate serine phosphorylation of Nanog downstream of an activated hyaluronan-CD44 signal to promote a chemoresistant phenotype in MCF7 breast carcinoma cells (16). Using mass spectrometry, murine Nanog was revealed to be phosphorylated by an unidentified kinase at S52, S65, S56/57, and S77/78 in HEK293 cells (17). Phosphorylation of Nanog enhanced its interaction with prolyl isomerase to prevent Nanog ubiquitination and degradation resulting in increased Nanog stability (17). Nanog was reported to be ubiquitinated at the PEST (rich in proline, glutamic acid, serine, and threonine) domain resulting in degradation through the proteasome pathway in embryonic stem cells (ESCs) (18). A recent study showed that focal

adhesion kinase (FAK) phosphorylates Nanog at Y35 and Y174 to modulate cell morphology and invasion in HEK293 cells (19). However, the functional significance of post-translational phosphorylation of Nanog remains to be fully elucidated in carcinomas.

In this study, we show, for the first time, that phosphorylation is a key mechanism to control Nanog-mediated Bmi1 regulation and tumorigenesis. Phosphopeptide mapping indicated that human PKCε phosphorylates human Nanog at multiple residues, T78, S79, S135, T200 and T280. Phosphorylation at T200 or T280 enhanced Nanog protein stability. Phosphorylation-insensitive T200A and T280A mutant Nanog showed a dominant-negative function and inhibited Nanog transcriptional activity through disruption of Nanog homodimerization, DNA binding, and p300 recruitment. Inactivation of endogenous Nanog with T200A or T280A mutant Nanog reduced Bmi1 and severely compromise tumorigenicity *in vitro* and *in vivo*. Recapitulation of Bmi1 was sufficient to rescue the Nanog inactivated loss-of-function phenotype. Our work reveals that Nanog directly regulates Bmi1 and an integrated Nanog-Bmi1 signaling network is essential for tumorigenesis.

Results

PKCε phosphorylates Nanog to enhance Nanog transcriptional activity

PKCε-mediated phosphorylation of Nanog was demonstrated in MCF10A breast carcinoma cells providing initial evidence that Nanog may be a substrate for PKCε (16). We determined if PKCε can directly phosphorylate Nanog *in vitro* and *in vivo*. As shown in Figure 1a, recombinant PKCε was demonstrated to directly phosphorylate recombinant Nanog *in vitro*. Mass spectrometry-phosphopeptide mapping analysis revealed that human Nanog is phosphorylated by human PKCε at multiple residues, T78, S79, S135, T200, and T280 (Figure 1b and Figure S1). To determine the functional significance of these phosphorylation sites, HEK293 cells were transfected to overexpress wildtype or phosphorylation-insensitive Nanog mutants and assessed for Nanog transcriptional activity. (Figure 1c) As expected, wildtype Nanog enhanced Nanog transcriptional activity by 64% (P<0.001). Nanog transcription activity was reduced by 42%, 41%, 47%, and 70% (P<0.001) in HEK293 cells expressing T78A, S79A, T200A, and T280A mutant Nanog, respectively. Interestingly, overexpression of S135A mutant Nanog had no effect on endogenous Nanog transcriptional activity in HEK293 cells.

We decided to focus our work on T200 and T280 for two key reasons. First, the phosphorylation-insensitive T200A and T280A mutant Nanog demonstrated a robust inhibitory effect on endogenous Nanog activity. Second, T200 and T280 are located in regions, tryptophan-rich (WR) domain and C-terminal domain 2 (CD2), critical for Nanog function. Several lines of evidence showed that the WR domain is essential for Nanog homodimerization and function (20, 21). In addition, the WR and CD2 domains were shown to cooperate to modulate Nanog transactivation activity (22, 23). We generated phosphorylation-specific antibodies to T200 and T280 of Nanog and validated their specificity using two different experimental approaches. Competition with 10X molar excess of the corresponding phosphopeptide used to generate the phospho-T200 or phospho-T280 Nanog antibody completely blocked the ability of the phospho-T200 or phospho-T280

Nanog antibody to detect phosphorylated Nanog in UMSCC74A cells (Figure 1d). In contrast, the phospho-T200 and phospho-T280 Nanog antibodies were able to detect phosphorylated Nanog in UMSCC74A cells in the presence of 10X molar excess of the corresponding nonphosphopeptide. As shown in Figure 1e, phospho-T200 Nanog antibody detected T200 phosphorylation in recombinant T280A mutant Nanog but not in recombinant T200A mutant Nanog. Moreover, phospho-T280 Nanog antibody detected T280 phosphorylation in recombinant T200A mutant Nanog but not in recombinant T280A mutant Nanog. These results confirm the specificity of the phospho-T200 and phospho-T280 Nanog antibody. HEK293 cells with expression of constitutive active-PKCε (CA-PKCε) were generated to confirm that Nanog is phosphorylated at T200 and T280 *in vivo*. HEK293/CA-PKCε cells had elevated levels of total Nanog and phosphorylated Nanog at T200 and T280. Moreover, Nanog transcriptional activity was enhanced by 2.4-fold (P<0.0001) in HEK293/CA-PKCε compared to control cells. These observations confirm that PKCε modulates Nanog transcriptional activity and demonstrate that Nanog is phosphorylated by PKCε at T200 and T280 *in vivo*.

Phosphorylation enhances Nanog protein stability

Our work showed that overexpression of PKCε is sufficient to enhance total and phosphorylated Nanog levels in HEK293 cells. Next, we determined if there is an association between PKCε and Nanog in HNSCC cell lines. SCC15, CAL27, and UMSCC74A HNSCC cells have increased PKCε levels compared to primary keratinocytes. This is consistent with our previous work demonstrating that PKCε levels are elevated in HNSCC (24). In comparison to primary keratinocytes, levels of phosphorylated Nanog at T200 and T280 and total Nanog were increased in HNSCC cell lines (Figure 2a). As shown in Figure 2b, genetic ablation of PKCε using an inducible shRNA-PKCε system in UMSCC74A cells resulted in a reduction in total Nanog and phosphorylated Nanog at T200 and T280. These observations reveal an association between total and phosphorylated Nanog levels suggesting that PKCε-mediated phosphorylation at T200 and/or T280 may enhance Nanog protein stability. UMSCC74 cells overexpressing wildtype/mutant Nanog were treated with cycloheximide (10 μM) for various time-points to determine the protein half-life of wildtype/mutant Nanog in HNSCC cells (Figure 2c). Wildtype Nanog was determined to have a protein half-life of 128 minutes. This is in line with published literature demonstrating that Nanog has a protein half-life of about 120 minutes in human embryonic stem cells (18). Phosphomimetic T200D and T280D mutant Nanog was more stable (P<0.01, n=3) whereas phosphosinsensitive T200A and T280A mutant Nanog was less stable (P<0.01, n=3) than wildtype Nanog. The protein half-lives of phosphomimetic T200D and T280D mutant Nanog was 172 and 157 minutes, respectively. In contrast, the protein half-life was 92 minutes for phosphoinsensitive T200A mutant Nanog and 76 minutes for phosphoinsensitive T280A mutant Nanog. Taken together, our results demonstrate that PKCε-mediated phosphorylation at T200 and T280 enhances Nanog protein stability in HNSCC.

Nanog regulates Bmi1 through promoter occupancy

We showed an association between PKCε, Nanog, and Bmi1 in HNSCC cells (Figures 2a and 2b). Several lines of evidence showed that Nanog and Bmi1 play similar roles in

tumorigenesis including modulation of the CIC population. However, the interplay between these key oncogenes remains to be examined. It is unclear if Nanog and Bmi1 promote tumorigenesis through independent pathways or through an integrated signaling network. In Figures 3a and 3b, Nanog-deficient UMSCC74A cells had lower Bmi1 protein levels and mRNA expression compared to UMSCC74A/shRNA-control cells further demonstrating a link between these two genes. Four putative Nanog binding sites, N1, N2, N3, and N4, were identified across an expanded Bmi1 promoter region (−4000 to +413) based on high sequence homology (>80% match) to the Nanog consensus binding motif suggesting that Nanog may directly regulate Bmi1 through promoter occupancy (Figures 3c and S2). ChIP analyses using UMSCC74A cells showed that Nanog is highly enriched at the N1 binding site located −220 to −210 with respect to the Bmi1 transcriptional start site (Figure 3c). As shown in Figure 3d, overexpression of wildtype Nanog enhanced Bmi1 promoter activity by 41% (P<0.005) in HEK293 cells using the 4.1 kb Bmi1 promoter fragment. Interestingly, Bmi1 promoter activity was increased by 46% (P<0.005) using a 0.9 kb Bmi1 promoter fragment containing only the N1 binding site. Deletion of the N1 site from the 0.9 kb Bmi1 promoter fragment (0.9 kb/ N1) attenuated Bmi1 promoter activity in control and Nanog-overexpressing HEK293 cells (P<0.005). These results indicate that the N1 site is the predominant Nanog binding site to transactivate the Bmi1 promoter. Electrophoretic mobility shift assay (EMSA) demonstrated that recombinant human wildtype Nanog binds to the N1 oligonucleotides but not the mutant N1 oligonucleotides (Figure 3e). Binding of Nanog to the labeled N1 oligonucleotides was reduced with the addition of excess amounts of unlabeled N1 oligonucleotides but not unlabeled mutant N1 oligonucleotides. Incubation with an anti-Nanog antibody resulted in a supershifted band further confirming that Nanog binds to the N1 site. Genetic ablation of Nanog in UMSCC74A cells decreased Bmi1 promoter activity by 30% (P<0.001) (Figure 3f). In addition, Bmi1 promoter occupancy by Nanog was decreased by 71% (P<0.0001) in Nanog-deficient UMSCC74A cells compared to UMSCC74A/shRNA-control cells (Figure 3g). Our work revealed for the first time that Nanog regulates Bmi1 through promoter occupancy and transactivation.

Phosphorylation of Nanog modulates homodimerization and Bmi1 promoter occupancy and transactivation

T200A and T280A mutant Nanog was shown to suppress endogenous Nanog activity in HEK293 cells. To determine if phosphorylation is a regulatory mechanism to control Nanog function in HNSCC cells, wildtype Nanog, T200A mutant Nanog, or T280A mutant Nanog were overexpressed in two HNSCC cell lines, UMSCC74A and CAL27 (Figure 4a). Wildtype Nanog enhanced Nanog transcriptional activity by 54% (P<0.0001) in UMSCC74A cells and 42% (P<0.0001) in CAL27 cells (Figure 4b). In addition, Bmi1 mRNA expression and protein levels were elevated in UMSCC74A/wildtype Nanog cells. In contrast, Nanog transcriptional activity was suppressed by 50% and 36% (P<0.0001) with T200A mutant Nanog and 83% and 43% (P<0.0001) with T280 mutant Nanog in UMSCC74A and CAL27, respectively. Enforced expression of T200A or T280A mutant Nanog reduced Bmi1 mRNA expression and protein levels compared to control cells (empty vector) providing further evidence that Bmi1 is downstream of Nanog (Figures 4a and 4c). As shown in Figure 4d, overexpression of wildtype Nanog enhanced Bmi1 promoter activity by 35% (P<0.001) in UMSCC74 cells. Deletion of the N1 site attenuated Bmi1 promoter

activation in control and wildtype Nanog-overexpressing HNSCC cells (P<0.001). Overexpression of T200A and T280A mutant Nanog reduced Bmi1 promoter activity in UMSCC74A by 39% (P<0.001) and 47% (P<0.001), respectively (Figure 4e). Consistent with our results in HEK293 cells, T200A and T280A mutant Nanog impart a dominant-negative effect on endogenous Nanog function in HNSCC cells. These results indicate that phosphorylation at T200 and T280 has other biological consequences independent of controlling Nanog protein stability.

To begin to understand how T200A and T280A mutant Nanog impart a dominant-negative effect, we determine the effect of phosphorylation on Nanog localization, homodimerization, DNA binding, and Bmi1 promoter occupancy. Similar to wildtype Nanog, T200A and T280 mutant Nanog was exclusively localized in the nucleus indicating that phosphorylation at T200 and T280 is not critical for trafficking Nanog to the nucleus (Figure 4f). As shown in Figure 4g, wildtype Nanog formed a dimeric complex whereas T200A and T280A mutant Nanog showed a complete defect in homodimerization. Interestingly, T200A and T280A mutant Nanog were able to dimerize with wildtype Nanog with varying affinities. Recombinant FLAG-tagged wildtype, T200A mutant, and T280A mutant Nanog were synthesized in HEK293 cells, purified, and assessed for DNA binding activity (Figures S3 and 4h). EMSA showed that wildtype Nanog binds to the Nanog TRE on the Bmi1 promoter in a dose-dependent manner. In contrast, T200A and T280A mutant Nanog showed a complete defect in DNA binding. Excess amount of T200A or T280A mutant Nanog disrupted the binding of wildtype Nanog to the Nanog TRE.

Next, we determined if phosphorylation of Nanog modulates p300 association and recruitment to the Bmi1 promoter. Nanog recruits p300 to co-occupy the promoters of target genes in ESCs (25). At this time, it is unclear how Nanog recruitment of p300 is regulated. We showed that endogenous Nanog forms a complex with endogenous p300 in UMSCC74A cells (Figure 4i). As expected, V5-tagged wildtype Nanog associated with endogenous p300 in UMSCC74A cells. In contrast, V5-tagged T200A and T280A mutant Nanog were unable to complex with p300. V5-tagged phosphorylation-mimetic T200D and T280D mutant Nanog showed an increased binding association with p300 compared to V5-tagged wildtype Nanog providing evidence that phosphorylation of Nanog is essential for p300 recruitment. ChIP analyses revealed that overexpression of V5-tagged wildtype Nanog enhance the occupancy of V5-tagged wildtype Nanog and endogenous p300 at the Bmi1 promoter (Figure 4j). In comparison to V5-tagged wildtype Nanog, V5-tagged T200A and T280A mutant Nanog showed a defect in Bmi1 promoter occupancy. Moreover, recruitment of p300 to the Bmi1 promoter was lower in cells overexpressing V5-tagged T200A or T280A mutant Nanog than control cells indicating that T200A and T280A mutant Nanog were able to block endogenous Nanog from recruiting p300. Our work demonstrates that phosphorylation is a key post-translational regulatory mechanism to control Nanog-mediated gene transcription through modulation of homodimerization, DNA binding, and p300 recruitment.

Pleiotropic anti-cancer effects of phosphorylation insensitive Nanog mutants

We determined the effects of the dominant-negative T200A and T280 mutant Nanog on HNSCC tumorigenicity *in vitro* and *in vivo* (Figure 5). Overexpression of the T200A mutant Nanog suppressed colony formation by 81%, cell invasion by 86%, and cell migration by 52% (P<0.01). Similarly, colony formation, cell invasion, and cell migration was blocked by 89%, 90%, and 62% with the T280A mutant Nanog, respectively (P<0.01). An accepted *in vitro* method to assess the CIC population is the tumorsphere formation assay. A significant reduction in tumorsphere formation efficiency and size were observed in UMSCC74A-200A and UMSCC74-280A compared to empty vector cells (UMSCC74A-control) indicting that the CIC population is depleted as a consequence of Nanog inactivation (Figure 5d). It should be noted that overexpression of wildtype Nanog enhanced the tumorigenicity of UMSCC74A cells; colony formation was increased by 74% (P<0.01), cell migration was increased by 124% (P<0.01), and tumorsphere formation efficiency was increased by 45% (P<0.01) (Figure S4). As shown in Figure 5e, UMSCC74A-control cells were highly tumorigenic and had a tumor incidence rate of 87.5% (14/16) in athymic nude mice. In contrast, *in vivo* tumorigenicity was severely compromised in UMSCC74A-T200A and UMSCC74A-T280A cells with tumor incidence of 12.5% (1/8) and 0% (0/8), respectively (*P*<0.0001). These results demonstrate that Nanog is a key regulator of tumorigenesis and inactivation of Nanog is sufficient to induce a potent anti-cancer response.

Bmi1 is essential for Nanog-induced tumorigenesis

The downstream signaling pathway essential for Nanog-induced tumorigenesis remains to be fully elucidated. Our results show that Nanog transactivates the Bmi1 promoter demonstrating a direct link between these two genes. Bmi1 was rescued in Nanog-inactivated HNSCC cells to determine if Bmi1 is indispensible for Nanog-mediated tumorigenesis (Figure 6). Recapitulation of Bmi1 was sufficient to rescue the loss-of-function defect in colony formation, cell invasion, and cell migration in Nanog-deficient and T280A mutant Nanog HNSCC cells. Additionally, Bmi1 enhanced the tumorsphere formation efficiency and tumorsphere diameter of Nanog-inactivated HNSCC cells (Figure 6e). Our results reveal that Bmi1 is responsible for the pleiotropic effects of Nanog on tumorigenesis.

Discussion

The Nanog protein is organized into 5 sub-domains, N-terminal domain (ND), homeodomain (HD), C-terminal domain 1 (CD1), tryptophan-rich (WR) domain, and C-terminal domain 2 (CD2). A recent study reports that the first 25 amino acids residues, in particular Ser2, in the ND of Nanog are crucial to maintain ESCs at an undifferentiated state (26). Several independent groups demonstrate that the WR domain is required for Nanog homodimerization (20, 21, 27). Homodimerization of Nanog is a major requirement for Nanog function in the context of ESC self-renewal (20, 21). In addition, dimeric Nanog constitute the core of Nanog protein complexes in ESCs further supporting the functional importance of Nanog homodimerization (21). The WR domain and CD2 of Nanog have potent transcriptional activity independently (22, 23). Furthermore, the CD2 and the WR domain are shown to cooperatively enhance Nanog transcriptional activity (23).

In this study, phosphopeptide mapping demonstrates that human PKCε phosphorylates human Nanog at five residues, T78, S79, S135, T200, and T280. T78/S79, S135, T200, and T280 are located in the ND, HD, WR domain, and CD2, respectively. Overexpression of phosphorylation-insensitive T78A, S79A, T200A, and T280A mutant Nanog inhibit endogenous Nanog activity. This observation shows that our phosphopeptide mapping approach has high fidelity to identify physiologically significant Nanog phosphorylation sites. We focused our work on T200 and T280 to examine the biological significance of post-translational phosphorylation in the WR and CD2 domains of Nanog. Phospho-T200 and T280 Nanog antibodies were developed and confirm that T200 and T280 are phosphorylated through a PKCε-mediated mechanism in HEK293 and HNSCC cells. Our data show that phosphorylation of Nanog at T200 and T280 controls Nanog protein stability, homodimerization, DNA binding, and recruitment of the co-activator p300. Similar to T200A and T280A mutations, T78A and S79A mutant Nanog impart a dominant-negative effect on endogenous Nanog activity. Ongoing work in our laboratory is to define the role of T78 and S79 phosphorylation on controlling Nanog function. Interestingly, endogenous Nanog activity is unaffected with the S135A mutant Nanog. Nanog has a nuclear localization signal (NLS; amino acids 136–141) in the HD that is necessary for nuclear localization (27). Since S135 is in close proximity to the NLS, we speculate that phosphorylation at S135 may facilitate the trafficking of Nanog from the cytosol to the nucleus. Our suggestion is in line with a study reporting that PKCε-mediated serine phosphorylation is required for Nanog to localize in the nucleus in MCF7 breast carcinoma cells (16). Additional work will be necessary to delineate the contribution of S135 phosphorylation as a requirement for Nanog nuclear localization.

It is indisputable that Bmi1, a member of the polycomb-repressive complex 1, regulates normal stem cell self-renewal. Accumulating literature provide compelling evidence that Bmi1 is intimately involved in tumorigenesis. Elevated Bmi1 is associated with poor prognosis in HNSCC and other epithelial malignancies (28–32). A Bmi1-driven stem cell-associated gene expression signature is highly predictive of disease recurrence, distant metastasis, and overall survival in numerous epithelial and non-epithelial malignancies (33). Bmi1 is overexpressed in CICs compared to non-CICs (34–36). Bmi1 regulates prostate stem cell self-renewal and ablation of Bmi1 with shRNA prevents fibroblast growth factor 10-induced prostate hyperplasia and attenuates prostate tumor growth in Pten-null prostate cells (37). Twist1-Bmi1 signaling axis represses E-cadherin and p16INK4a to induce epithelial-mesenchymal transition (EMT) and enhance cancer initiating potential (38). A recent study demonstrates that Twist1 cooperates with Bmi1 to repress let-7i leading to enhance Rac1 activation, cell migration, and cancer initiating potential (39). Interestingly, suppression of let-7i did not promote EMT indicating that Twist1 and Bmi1 can modulate tumor phenotype in EMT-dependent and independent manner (39). Based on these studies, it is clear that Bmi1 is essential to promote tumorigenesis, however, the molecular mechanisms leading to Bmi1 dysregulation remains to be elucidated. Our results show that Nanog intimately regulates Bmi1 through direct promoter occupancy and transactivation. Nanog-deficient or Nanog-inactivated HNSCC cells have lower Bmi1 levels and moreover, recapitulation of Bmi1 in these cells is sufficient to rescue the loss-of-function phenotype.

Thus, our work reveals a clear hierarchy between these two genes and furthermore, demonstrates that the Nanog-Bmi1 signaling axis is indispensible for tumorigenesis.

During the review process of this manuscript, a group reported that Nanog occupies the BS1 site (−3821) on the murine Bmi1 promoter to repress Bmi1 expression to maintain pluripotency in murine ESCs (40). This finding is inconsistent with our data demonstrating that Nanog enhances Bmi1 expression through direct promoter occupancy at the N1 site in HNSCC. The difference in Bmi1 regulation by Nanog between these two studies simply may be due to the use of different species (murine vs. human) and/or model cell systems (ESCs vs. HNSCC cells). Sequence alignment of the extended human and murine Bmi1 promoters identified only three discrete regions of similarity; −382 to −7 (human) and −429 to −31 (murine) has 85% identity and 11% gaps, −1159 to −910 (human) and −1279 to −1035 (mouse) has 82% identity and 4% gaps, and −3137 to −1986 (human) and −3340 to −2133 (mouse) has 76% identity and 8% gaps. Interestingly, the murine BS1 site is not conserved in the human Bmi1 promoter whereas the human N1 site is conserved in the murine Bmi1 promoter (−254 to −244). Lavial *et al.* reported eight putative Nanog binding sites over the murine Bmi1 locus, however, their analysis failed to identify the conserved N1 site (40). A caveat of their work is that a truncated Bmi1 promoter-luciferase construct without the N1 site was used to provide the key evidence to show that Nanog represses Bmi1 promoter activity. Thus, the effect of murine Nanog on an extended murine Bmi1 promoter that spans the N1 site remains to be determined. In addition, it is unclear if the N1 site is accessible for occupancy by murine Nanog in ESCs. Our results clearly indicate that Nanog positively regulates Bmi1 in HNSCC. This observation is in line with several independent reports demonstrating that Nanog and Bmi1 are elevated in carcinoma cells with CIC properties (14, 41–43). In this study, ChIP data showed that human Nanog is highly enriched at the N1 site in HNSCC. Human Nanog is able to enhance the activity of a truncated human Bmi1 promoter containing only the N1 site (0.9 kb promoter) to a similar extent as the extended 4.1 kb human Bmi1 promoter. Moreover, deletion of the N1 site abrogated the transactivation of the human Bmi1 promoter by human Nanog in HNSCC cells. Taken together, our data show that the N1 site in the Bmi1 promoter is the predominant human Nanog transcriptional response element in HNSCC cells.

Inactivation of endogenous Nanog in HNSCC cells with dominant-negative T200A or T280 mutant Nanog is sufficient to attenuate the pleiotropic, pro-oncogenic effects of Nanog *in vitro* and *in vivo*. We identify several molecular mechanisms responsible for the dominant-negative effects of the T200A and T280 mutant Nanog. T200A and T280 mutant Nanog show a gross defect in homodimerization and DNA binding suggesting that a dimeric Nanog complex may be a required step prior to binding to the Nanog consensus response element. Interestingly, T200A and T280A mutant Nanog is able to dimerize with wildtype Nanog. It should be noted that the T280A mutant Nanog is as efficient as wildtype Nanog whereas the T200A mutant Nanog is much less efficient to form a dimeric complex with wildtype Nanog. These observations suggest that phosphorylation of T200 in both monomers may be necessary to maximally promote dimeric Nanog complex formation. Furthermore, it appears that phosphorylation of T280 in both monomers may not be a requirement for Nanog homodimerization since a defect in dimerization between wildtype Nanog and the T280A

mutant Nanog is not observed. The addition of excess T200A or T280A mutant Nanog blocks wildtype Nanog from binding to the consensus Nanog response element in the Bmi1 promoter. Moreover, ChIP studies indicate that V5-tagged T200A and T280A mutant Nanog have a defect in Bmi1 promoter occupancy compared to V5-tagged wildtype Nanog. These results provide evidence that dimeric T200A or T280A mutant:wildtype Nanog has a lower DNA binding affinity than dimeric wildtype:wildtype Nanog since T200A and T280A mutant Nanog are unable to homodimerize and bind to DNA. Thus, a plausible explanation for the dominant-negative effect of the T200A and T280A mutant Nanog is that the T200A and T280A mutant Nanog is squelching endogenous Nanog by preventing the formation of a fully functional wildtype:wildtype Nanog homodimer.

Our data also support the notion that phosphorylation of Nanog is essential for p300 association and recruitment to the Bmi1 promoter. p300 is a transcriptional co-activator recruited by numerous transcriptional factors to facilitate target gene transcription. Genome-wide promoter occupancy analysis in ESCs reveals that p300 and the core ESC transcription factors, Nanog, Oct4, and Sox2, co-occupy the promoter of various genes involved in pluripotency (25). Genetic depletion of Nanog, Oct4, or Sox2 results in a reduction in p300 binding indicating that the core ESC transcription factors recruit p300 to the promoter regions of target genes (25). In direct support, overexpression of V5-tagged wildtype Nanog results in an increase in co-occupancy of V5-tagged wildtype Nanog and endogenous p300 in HNSCC cells. Overexpression of V5-tagged T200A or T280A mutant Nanog inhibits the recruitment of p300 to the Bmi1 promoter by 50% compared to empty vector control. It is possible that the residual p300 signal may be a result of incomplete displacement of endogenous dimeric wildtype:wildtype Nanog by T200A or T280A mutant Nanog from the Bmi1 promoter. We show that T200A and T280A mutant Nanog is defective in p300 binding, whereas, the T200D and T280D mutant Nanog show an increase in p300 binding demonstrating that phosphorylation of Nanog is a necessary step for p300 association. Based on these results, an alternate explanation for the decrease in p300 promoter occupancy in HNSCC cells overexpressing V5-tagged T200A or T280A mutant Nanog is that dimeric T200A or T280A mutant:wildtype Nanog is not as efficient as dimeric wildtype:wildtype Nanog to recruit p300 to target genes.

In summary, our work reveals a novel regulatory mechanism to control Nanog transcriptional activity. Post-translational phosphorylation is essential for Nanog stability, homodimerization, DNA binding, and p300 recruitment. Bmi1 is revealed to be downstream of Nanog and indispensible for Nanog-induced tumorigenesis. Based on our results, we propose a model for the PKCε-Nanog-Bmi1 signaling module in tumorigenesis (Figure 7). PKCε phosphorylates Nanog at T200 and T280 to enhance Nanog stability, homodimerization and Bmi1 promoter occupancy. Subsequently, the p300 co-activator is recruited to facilitate Bmi1 promoter transactivation. Our model suggests that the PKCε-Nanog-Bmi1 axis may be disrupted at three key steps; PKCε phosphorylation of Nanog, Nanog homodimerization, and Nanog-mediated p300 recruitment. Thus, development of inhibitors to block these critical points may yield a potent collection of molecularly-targeted anti-cancer therapeutics.

Materials and Methods

Cell lines

HEK293, SCC15, and CAL27 were purchased from ATCC (Manass, VA). UMSCC74A was obtained from Dr. Thomas Carey at the University of Michigan. All cell lines were maintained in a humidified atmosphere of 5% CO_2 at 37°C. SCC15 cells were grown in a 1:1 mixture of Ham's F-12 and DMEM supplemented with 0.4 mg/mL hydrocortisone, 10% FBS, 100 mg/mL streptomycin and 100 U/mL penicillin. HEK293, CAL27 and UMSCC74A cells were grown in DMEM containing 10% FBS, 100 mg/mL streptomycin and 100 U/mL penicillin.

In vitro kinase assay

Recombinant human wildtype PKCε (GenWay Biotech Inc., San Diego, CA) was incubated with recombinant human wildtype Nanog in kinase buffer (24 mM Tris (pH 7.4), 0.5 mM EDTA, 0.5 mM EGTA, 10 mM β-mercaptoethanol, 1 μg/ml leupeptin, 1 μg/ml aprotinin, and 50 μg/ml PMSF) containing PKC activators, phosphatidylserine and diacylglycerol, and ATP for 30 minutes at 25°C. Subsequently, termination buffer consisting of 7.5 M guanidine-HCl was added to stop the reaction. The incubation reaction was separated by SDS-PAGE and visualized with Pro-Q Diamond Phosphoprotein Stain and SYPRO Ruby Total Protein Stain (Invitrogen, Carlsbad, CA).

Phosphopeptide mapping

Nanog was phosphorylated by PKCε *in vitro* and then subjected to proteolytic enzyme digestion. Following digestion, the resulting peptide sample was acidified to 0.5% trifluroacetic acid concentration and stored at −20°C until further analyzed. The digested Nanog protein was analyzed by reverse-phase nanoscale LC-MS^E using a Waters QTof Premier mass spectrometry system. To aid recovery of phosphopeptides from the UPLC system, EDTA and diammonium phosphate was added to sample for a final concentration of 25 mM each and 11–25 ng of digested protein was analyzed. Peptides were separated using acetonitrile/water mobile phases containing 0.1% formic acid on a Waters NanoAcquity UPLC system employing a 300 μm ID x 20 mm C-18 5 μm particle Symmetry trap column and a 75 μm ID x 150 mm C-18 1.7 μm BEH analytical column. Peptides were trapped for 15 minutes at 3 μL/min followed by gradient elution using 0–28% acetonitrile in 40 minutes through the analytical column at 300 nL/min. ESI was conducted at approximately 3.3 kV using in house prepared spray emitters. The Qtof Premier mass spectrometer was programmed to collect alternate scan MS^E data as previously described (44, 45). Glu-fibrinopeptide at a concentration of 200 fmol/μL in 25% acetonitrile/water/0.1% formic acid was introduced as a lockspray calibrant through a second ESI probe at 0.5 μL/min using an auxiliary UPLC pump. Lockspray data was collected for 1 second every 30 seconds over a 65 minute analysis.

Following an LC-MS^E analysis, data processing was performed using Waters PLGS software version 2.3 build 23 using the following parameters: low energy threshold 100 counts, high energy threshold 10 counts, and an intensity threshold of 1000 counts. Data processing combined the signal intensity of all charge states generated from a given peptides

into singly charged MH$^+$ values and determined the peak apex for both low energy precursors and all fragment ions within the vicinity of the precursor. This lockmass corrected, accurate mass data was used in two ways. First, the data was used to search Human RefSeq database version 17 within PLGS software using the following search parameters: peptide and fragment tolerance was automatic, the minimum fragment Ion matches per peptide was 3, the minimum fragment ions per protein was 7, the minimum peptides matches per protein was 1, missed cleavages was 2, the false positive rate was 4%, modifications allowed were Acetyl N-term, Carbamidomethyl-C, Carbamyl N-term and phosphorylation at STY. Second, low energy precursor MH$^+$ data was copied into Excel and compared to MH$^+$ values calculated for predicted Nanog trypsin, chymotrypsin, or Glu-C protease peptides bearing up to 4 phosphate groups (Lighthouse Data, GPMAW version 8.00sr1, Odense, Denmark).

Experimental MH+ masses that matched within 0.03 Da of GPMAW calculated values were evaluated manually in PLGS or Masslynx Protein/Peptide Editor software. Possible assignment was made when peptide identification was positive when greater than 3 accurate mass product ions could be assigned to a peptide sequence. Confident site specific phosphorylation also used these criteria but further required fragment ions including phosphorylated serine or threonine amino acids.

Generation of PKCε, Nanog, and Bmi1 overexpressing cells

Human Nanog and PKCε cDNA was cloned into pcDNA3.1 expression vector (Invitrogen) by PCR from a human cDNA library (Clontech, Mountain View, CA). Myc-DDK-tagged Nanog and Bmi1 expression vectors (pCMV6) were purchased from OriGene (Rockville, MD). CA-PKCε (A159E) and T78, S79, S135, T200A, T200D, T280A, and T280D mutant Nanog were generated using the QuikChange Lightning kit (Agilent Technologies, Inc., Santa Clara, CA). Cells were transfected with various expression vectors using Lipofectamine2000. Stable polyclonal cell populations were generated by selection using appropriate antibiotics (Invitrogen).

Generation of Nanog-deficient and PKCε-deficient HNSCC cells

UMSCC74A cells were transduced with pGIPZ shRNA-control or shRNA-Nanog lentiviral particles (MOI 20; Open Biosystems, Huntsville, AL) for 6 hours and subsequently cultured in complete growth media for 48 hours. Polyclonal populations of UMSCC74A/shRNA-control and UMSCC74A/shRNA-Nanog cells were generated by selection in puromycin. UMSCC74A cells were transduced with pTRIPZ shRNA-PKCε lentiviral particles (MOI 20; Open Biosystems) for 12 hours and subsequently cultured in complete growth media for 48 hours. Polyclonal populations of UMSCC74A/inducible shRNA-PKCε cells were generated by selection in puromycin. UMSCC74A/inducible shRNA-PKCε cells were induced with 5 μg/ml of doxycycline for 48 hours for all experiments.

Generation of recombinant wildtype and mutant Nanog

HEK293 cells were transfected with pCMV6/Nanog-wildtype, pCMV6/Nanog-T200A, or pCMV6/Nanog-T280A using Lipofectamine2000. Cells lysates were extracted and recombinant DDK-tagged wildtype/mutant Nanog was purified by competition with 3X

FLAG peptide using the FLAG Purification Kit (Sigma-Aldrich, CELL MM2). Recombinant wildtype/mutant Nanog was separated by SDS-PAGE and visualized with SYPRO Ruby Total Protein Stain to assess protein purity.

Western blot analysis

Whole cell lysates were mixed with Laemmli loading buffer, boiled, separated by SDS-PAGE, and transferred to a nitrocellulose membrane. Subsequently, immunoblot analyses were performed using antibodies specific to PKCε (Santa Cruz Biotechnology, Santa Cruz, CA), Nanog (Santa Cruz Biotechnology), V5 (Invitrogen), FLAG (Origene), or GAPDH (Cell Signaling Technology, Danvers, MA). The signal was developed with ECL (Thermo Fisher Scientific) after incubation with appropriate secondary antibodies.

Production of phospho-specific Nanog antibodies

Phospho-T200 and phospho-T280 Nanog antibodies were developed in collaboration with 21st Century Biochemicals (Marlboro, MA) by immunizing rabbits with synthetic peptide corresponding to residues surrounding human Nanog T200, PMWSNQ[pT]WNNSTW-amide, or T280, LNVIQQ[pT]TRYFST-amide. The peptides were synthesized with N-terminal cysteine residue and coupled to MBS for immunization. The antibodies were affinity purified from rabbit antisera using a sequential purification process with protein A columns to purify immunoglobulins followed by specific immunodepletion using nonphosphopeptide columns and affinity purification using phosphopeptide columns.

Nanog transcriptional activity

HEK293, CAL27, or UMSCC74A cells were transduced (MOI 10:1) with Cignal Lenti Nanog Reporter (SABiosciences, Frederick, MD). The Cignal Lenti Nanog Reporter contains tandem repeats of the Nanog transcriptional response element (TRE) upstream of Firefly luciferase gene. Stable polyclonal HEK293/CAL27/UMSCC74A-Nanog-TRE cells were generated by selection in puromycin for 14 days. HEK293-Nanog-TRE cells were transfected with pcDNA3.1/control (empty vector), pcDNA3.1/CA-PKCε, pcDNA3.1/Nanog-wildtype, pcDNA3.1/Nanog-T78A, pcDNA3.1/Nanog-S79A, pcDNA3.1/Nanog-S135A pcDNA3.1/Nanog-T200A, or pcDNA3.1/T280A using Lipofectamine2000 and selected in G418 to generate stable polyclonal population. CAL27/UMSCC74A-Nanog-TRE cells were transfected with pcDNA3.1/control (empty vector), pcDNA3.1/Nanog-wildtype, pcDNA3.1/Nanog-T200A, or pcDNA3.1/Nanog-T280A using Lipofectamine2000 and selected in G418 to generate stable polyclonal population. Cell lysates were prepared and measure for Firefly luciferase activity using a luminometer.

Bmi1 promoter activity

The 4.1 kb (−3733 to +413) Bmi1 promoter was amplified from UMSCC74A genomic DNA using the primers, 5′-CCGCTCGAGTCATGGAGCCGGTTACCCTAAACT-3′ (Forward) and 5′-CCCAAGCTTAAATGAATGCGAGCCAAGCGGCC-3′ (Reverse), subcloned into the pGL4-Renilla luciferase plasmid (Promega, Madison, WI), and verified by DNA sequencing. A 0.9 kb (−532 to +393) Bmi1 promoter-Renilla luciferase plasmid containing only the N1 TRE was purchased (SwitchGear Genomics, Menlo Park, CA). Deletion of the

N1 TRE (0.9 kb/ N1) in the 0.9-kb Bmi1 promoter was performed with the QuikChange II XL Site-Directed Mutagenesis Kit (Stratagene, La Jolla, CA) using the primers, 5′-GGGCCTGACTACACCCCCTTAAGGAATGAG-3′ (Forward) and 5′-CTCATTCCTTAAGGGGGTGTAGTCAGGCCC-3′ (Reverse), and verified by DNA sequencing. Cells were co-transfected with the 4.1 kb, 0.9 kb, or 0.9 kb/ N1 Bmi1 promoter-Renilla luciferase and the CMV-Firefly luciferase (Promega) plasmid (100:1 ratio) using FuGENE HD (Promega). After 48 hours, cells were washed with PBS, lysed in passive lysis buffer, and measured for Renilla/Firefly luciferase activities in a luminometer using the Dual-Light System (Applied Biosystems, Foster City, CA). Bmi1 promoter Renilla luciferase activities were normalized with Firefly luciferase activities to control for transfection efficiency.

Electrophoretic mobility shift assay

Electrophoretic mobility shift assays were carried out using 3′-biotinylated double-stranded DNA probes (Invitrogen). The sequence for the N1 TRE on the Bmi1 promoter is 5′-ACCGACACTAATTCCCAGG-3′. The sequence for the mutant N1 TRE is 5′-ACCGACAC**A**AA**A**TCCCAGG-3′. Equimolar amounts of complementary strands were mixed and heated to 95°C followed by gradual cooling to ambient temperature over at least 5 hours to anneal the probes. Double-stranded DNA probes (40 fmol) were mixed with 10 ng of recombinant wildtype Nanog or 2 µg of nuclear extract from UMSCC74A cells in 20 µl reaction buffer containing 10 mM Hepes, pH 7.9, 50 mM KCl, 10 mM NaCl, 5 mM MgCl$_2$, 2.5% glycerol, 1 mM DTT and 0.4 mM ethylenediaminetetraacetic acid, and incubated for 20 min at room temperature. The bound protein:DNA complexes were separated at 10°C on a prerun 6% polyacrylamide gel in 0.5X TBE and transferred to a positive-charged nylon membrane. The signal was developed with using the LightShift Chemiluminescent EMSA Kit (Thermo Fisher Scientific). For the competition experiments, 1X or 10X molar excess of unlabeled wildtype or mutant N1 oligonucleotides were added prior to incubation with the labeled wildtype N1 oligonucleotides. For the supershift assay, anti-IgG or anti-Nanog antibodies (Cell Signaling Technology) was added to the reaction mixture and incubated at 4°C for 30 min prior to the addition of the labeled wildtype N1 oligonucleotides.

Cell invasion, migration, and proliferation

Cell invasion was determined using the BD Biocoat Matrigel Invasion Chamber (BD Biosciences). Cells were harvested and re-suspended in serum free DMEM medium. An aliquot (4×10^4 cells) of the prepared cell suspension was carefully added into the chamber and incubated for 24 hours at 37°C. The non-invaded cells were carefully removed from the interior of the inserts with a cotton-tipped swab. The inserts were then stained with 0.25% crystal violet in 25% methanol, washed, and air dried. Cell migration was determined using the wound-healing assay. Confluent monolayer cells were scratched with a pipette tip, rinsed with PBS, and fresh culture media were added. Wounds areas were marked and photographed at different time points using a phase-contrast microscope. Cell proliferation was assessed using the MTT reagent to detect metabolic active cells (Roche Molecular Biochemicals, Nutley, NJ). Absorbance was measured at 570nm in the Spectra Max 190 ELISA reader (Molecular Devices, Sunnyvale, CA) after overnight incubation.

Clonogenic survival

Cells were harvested, and re-suspended in complete growth media. Cells were seeded onto 6-well plates and allowed to grow until visible colonies formed (7 days). Cell colonies were fixed with cold methanol, stained with 0.25% crystal violet in 25% methanol, washed and air-dried.

Tumorsphere formation efficiency

Tumorspheres were generated from HNSCC cell lines grown in serum-free defined medium consisting of KSF medium (Invitrogen) supplemented with epidermal growth factor (20 ng/mL), basic fibroblast growth factor (20 ng/mL), insulin (100 ng/mL), and hydrocortisone (400 ng/mL) in low-attachment plates (Corning Incorporated, Corning, NY). Images were captured using the Nikon Eclipse 80i upright fluorescence microscope equipped with a digital camera and analyzed using the NIS-Elements software (Nikon Instruments Inc., Melville, NY). Tumorsphere formation efficiency was calculated as the number of tumorspheres (50 μm in diameter) formed in 7 days divided by the initial number of single cells seeded.

Tumor incidence in athymic nude mice

Athymic nude mice were purchased from the National Cancer Institute (Bethesda, MD). All mouse procedures were approved by the Animal Care and Use Committee at the Ohio State University. UMSCC74A-control, UMSCC74A-T200A, and UMSCC74A-T280A cells (1×10^6 cells) were suspended in DMEM (50:50 Matrigel) and implanted subcutaneously in the flanks of 6-week old athymic nude mice. Tumor incidence was monitored for 68 days post-implantation. Palpable tumors of any size were considered positive for tumor incidence.

Chromatin immunoprecipitation

Chromatin immunoprecipitation (ChIP) were performed using the SimpleChIP® Enzymatic Chromatin IP Kit (Cell Signaling). Briefly, cells were cross-linked with 1% formaldehyde for 10 min at room temperature. Cross-linking reactions were stopped by the addition of a 1/10 volume of 10X glycine and incubated at room temperature for 5 minutes. The cells were washed with ice-cold PBS, collected, and then nuclei were collected after cell lysis. Micrococcal nuclease was added to the nuclei suspension to digest the DNA for 20 min at 37°C and subsequent, 0.5 M EDTA was added to stop the reaction. Sheared chromatin was collected after sonication. Chromatin extracts containing DNA fragments with an average size of 500 basepairs were immunoprecipitated using anti-Nanog (Santa Cruz Biotechnology), anti-p300 (Millipore), anti-V5 (Invitrogen), or anti-IgG (Cell Signaling) antibody. Quantitative real-time PCR analyses were performed using the ABI PRISM 7900 Sequence Detection System and RT^2 SYBR Green qPCR Master Mix (SABiosciences) with primers designed to amplify select regions of the Bmi1 promoter; N1: 5′-GGCCTGACTACACCGACACT-3′ (Forward) and 5′-CTCCAAAATGGCTCGGAGT-3′ (Reverse); N2: 5′-GAGGGAAAGATACTGCCCAAG-3′ (Forward) and 5′-CACGAACTCAGATCCAAACAAA-3′ (Reverse); N3: 5′-AGCGTTTCTTGTTGCGTGTT-3′ (Forward) and 5′-TGTACCTGTAATTGTTCCATGCT-3′ (Reverse); N4: 5′-

TGTTATATTTTCTTTGGGGGCTA-3′ (Forward) and
5′TGAGCAACAAGATCAAGTGAAAA-3′ (Reverse).

Immunoprecipitation

Whole cell lysates were immunoprecipitated with anti-p300 antibody (Millipore), anti-DDK antibody (Abcam), or anti-IgG antibody (Cell Signaling) overnight, followed by anti-IgG beads. Subsequently, the immunoprecipitated protein complexes were solubilized in SDS sample buffer, electrophoresed, and blotted onto nitrocellulose membrane. Subsequently, immunoblot analyses were performed using antibodies specific to V5 (Invitrogen) or Nanog (Santa Cruz Biotechnology). The signal was developed with ECL (Thermo Fisher Scientific) after incubation with appropriate secondary antibodies.

Statistical analysis

Data were analyzed by two-tailed Student's *t*-test. P-value<0.05 were considered significant.

Supplementary Material

Refer to Web version on PubMed Central for supplementary material.

Acknowledgments

References

1. Niwa H, Miyazaki J, Smith AG. Quantitative expression of Oct-3/4 defines differentiation, dedifferentiation or self-renewal of ES cells. Nat Genet. 2000 Apr; 24(4):372–6. [PubMed: 10742100]

2. Mitsui K, Tokuzawa Y, Itoh H, Segawa K, Murakami M, Takahashi K, et al. The homeoprotein Nanog is required for maintenance of pluripotency in mouse epiblast and ES cells. Cell. 2003 May 30; 113(5):631–42. [PubMed: 12787504]

3. Masui S, Nakatake Y, Toyooka Y, Shimosato D, Yagi R, Takahashi K, et al. Pluripotency governed by Sox2 via regulation of Oct3/4 expression in mouse embryonic stem cells. Nat Cell Biol. 2007 Jun; 9(6):625–35. [PubMed: 17515932]

4. Torres J, Watt FM. Nanog maintains pluripotency of mouse embryonic stem cells by inhibiting NFkappaB and cooperating with Stat3. Nat Cell Biol. 2008 Feb; 10(2):194–201. [PubMed: 18223644]

5. Zhang P, Andrianakos R, Yang Y, Liu C, Lu W. Kruppel-like factor 4 (Klf4) prevents embryonic stem (ES) cell differentiation by regulating Nanog gene expression. J Biol Chem. 2010 Mar 19; 285(12):9180–9. [PubMed: 20071344]

6. Yu CC, Chen YW, Chiou GY, Tsai LL, Huang PI, Chang CY, et al. MicroRNA let-7a represses chemoresistance and tumourigenicity in head and neck cancer via stem-like properties ablation. Oral Oncol. 2011 Mar; 47(3):202–10. [PubMed: 21292542]

7. Chiou SH, Yu CC, Huang CY, Lin SC, Liu CJ, Tsai TH, et al. Positive correlations of Oct-4 and Nanog in oral cancer stem-like cells and high-grade oral squamous cell carcinoma. Clin Cancer Res. 2008 Jul 1; 14(13):4085–95. [PubMed: 18593985]

8. Han J, Zhang F, Yu M, Zhao P, Ji W, Zhang H, et al. RNA interference-mediated silencing of NANOG reduces cell proliferation and induces G0/G1 cell cycle arrest in breast cancer cells. Cancer Lett. 2012 Feb 28.

9. Chiou SH, Wang ML, Chou YT, Chen CJ, Hong CF, Hsieh WJ, et al. Coexpression of Oct4 and Nanog enhances malignancy in lung adenocarcinoma by inducing cancer stem cell-like properties and epithelial-mesenchymal transdifferentiation. Cancer Res. 2010 Dec 15; 70(24):10433–44. [PubMed: 21159654]

10. Meng HM, Zheng P, Wang XY, Liu C, Sui HM, Wu SJ, et al. Overexpression of nanog predicts tumor progression and poor prognosis in colorectal cancer. Cancer Biol Ther. 2010 Feb 16.9(4)

11. Jeter CR, Badeaux M, Choy G, Chandra D, Patrawala L, Liu C, et al. Functional evidence that the self-renewal gene NANOG regulates human tumor development. Stem Cells. 2009 May; 27(5): 993–1005. [PubMed: 19415763]

12. Zbinden M, Duquet A, Lorente-Trigos A, Ngwabyt SN, Borges I, Ruiz i Altaba A. NANOG regulates glioma stem cells and is essential in vivo acting in a cross-functional network with GLI1 and p53. EMBO J. 2010 Aug 4; 29(15):2659–74. [PubMed: 20581802]

13. Tsai LL, Yu CC, Chang YC, Yu CH, Chou MY. Markedly increased Oct4 and Nanog expression correlates with cisplatin resistance in oral squamous cell carcinoma. J Oral Pathol Med. 2011 Sep; 40(8):621–8. [PubMed: 21342274]

14. Germann M, Wetterwald A, Guzman-Ramirez N, van der Pluijm G, Culig Z, Cecchini MG, et al. Stem-Like Cells with Luminal Progenitor Phenotype Survive Castration in Human Prostate Cancer. Stem Cells. 2012 Mar 21.

15. Bourguignon LY, Earle C, Wong G, Spevak CC, Krueger K. Stem cell marker (Nanog) and Stat-3 signaling promote MicroRNA-21 expression and chemoresistance in hyaluronan/CD44-activated head and neck squamous cell carcinoma cells. Oncogene. 2012 Jan 12; 31(2):149–60. [PubMed: 21685938]

16. Bourguignon LY, Spevak CC, Wong G, Xia W, Gilad E. Hyaluronan-CD44 interaction with protein kinase C(epsilon) promotes oncogenic signaling by the stem cell marker Nanog and the Production of microRNA-21, leading to down-regulation of the tumor suppressor protein PDCD4, anti-apoptosis, and chemotherapy resistance in breast tumor cells. J Biol Chem. 2009 Sep 25; 284(39):26533–46. [PubMed: 19633292]

17. Moretto-Zita M, Jin H, Shen Z, Zhao T, Briggs SP, Xu Y. Phosphorylation stabilizes Nanog by promoting its interaction with Pin1. Proc Natl Acad Sci U S A. 2010 Jul 27; 107(30):13312–7. [PubMed: 20622153]

18. Ramakrishna S, Suresh B, Lim KH, Cha BH, Lee SH, Kim KS, et al. PEST motif sequence regulating human NANOG for proteasomal degradation. Stem Cells Dev. 2012 Sep; 20(9):1511–9. [PubMed: 21299413]

19. Ho B, Olson G, Figel S, Gelman I, Cance WG, Golubovskaya VM. Nanog Increases Focal Adhesion Kinase (FAK) Promoter Activity and Expression and Directly Binds to FAK Protein to Be Phosphorylated. J Biol Chem. 2012 May 25; 287(22):18656–73. [PubMed: 22493428]

20. Mullin NP, Yates A, Rowe AJ, Nijmeijer B, Colby D, Barlow PN, et al. The pluripotency rheostat Nanog functions as a dimer. Biochem J. 2008 Apr 15; 411(2):227–31. [PubMed: 18290762]

21. Wang J, Levasseur DN, Orkin SH. Requirement of Nanog dimerization for stem cell self-renewal and pluripotency. Proc Natl Acad Sci U S A. 2008 Apr 29; 105(17):6326–31. [PubMed: 18436640]

22. Pan G, Pei D. The stem cell pluripotency factor NANOG activates transcription with two unusually potent subdomains at its C terminus. J Biol Chem. 2005 Jan 14; 280(2):1401–7. [PubMed: 15502159]

23. Do HJ, Lee WY, Lim HY, Oh JH, Kim DK, Kim JH, et al. Two potent transactivation domains in the C-terminal region of human NANOG mediate transcriptional activation in human embryonic carcinoma cells. J Cell Biochem. 2009 Apr 15; 106(6):1079–89. [PubMed: 19229867]

24. Pan Q, Bao LW, Teknos TN, Merajver SD. Targeted disruption of protein kinase C epsilon reduces cell invasion and motility through inactivation of RhoA and RhoC GTPases in head and neck squamous cell carcinoma. Cancer Res. 2006 Oct 1; 66(19):9379–84. [PubMed: 17018591]

25. Chen X, Xu H, Yuan P, Fang F, Huss M, Vega VB, et al. Integration of external signaling pathways with the core transcriptional network in embryonic stem cells. Cell. 2008 Jun 13; 133(6): 1106–17. [PubMed: 18555785]

26. Das S, Jena S, Levasseur DN. Alternative splicing produces Nanog protein variants with different capacities for self-renewal and pluripotency in embryonic stem cells. J Biol Chem. 2011 Dec 9; 286(49):42690–703. [PubMed: 21969378]

27. Chang DF, Tsai SC, Wang XC, Xia P, Senadheera D, Lutzko C. Molecular characterization of the human NANOG protein. Stem Cells. 2009 Apr; 27(4):812–21. [PubMed: 19350681]

28. Song LB, Zeng MS, Liao WT, Zhang L, Mo HY, Liu WL, et al. Bmi-1 is a novel molecular marker of nasopharyngeal carcinoma progression and immortalizes primary human nasopharyngeal epithelial cells. Cancer Res. 2006 Jun 15; 66(12):6225–32. [PubMed: 16778197]

29. Vrzalikova K, Skarda J, Ehrmann J, Murray PG, Fridman E, Kopolovic J, et al. Prognostic value of Bmi-1 oncoprotein expression in NSCLC patients: a tissue microarray study. J Cancer Res Clin Oncol. 2008 Sep; 134(9):1037–42. [PubMed: 18264721]

30. Vormittag L, Thurnher D, Geleff S, Pammer J, Heiduschka G, Brunner M, et al. Co-Expression of Bmi-1 and Podoplanin Predicts Overall Survival in Patients with Squamous Cell Carcinoma of the Head and Neck Treated with Radio(Chemo)Therapy. International Journal of Radiation Oncology Biology Physics. 2009 Mar 1; 73(3):913–8.

31. Hayry V, Makinen LK, Atula T, Sariola H, Makitie A, Leivo I, et al. Bmi-1 expression predicts prognosis in squamous cell carcinoma of the tongue. Br J Cancer. 2010 Mar 2; 102(5):892–7. [PubMed: 20145620]

32. Li J, Gong LY, Song LB, Jiang LL, Liu LP, Wu J, et al. Oncoprotein Bmi-1 renders apoptotic resistance to glioma cells through activation of the IKK-nuclear factor-kappaB Pathway. Am J Pathol. 2010 Feb; 176(2):699–709. [PubMed: 20035051]

33. Glinsky GV, Berezovska O, Glinskii AB. Microarray analysis identifies a death-from-cancer signature predicting therapy failure in patients with multiple types of cancer. J Clin Invest. 2005 Jun; 115(6):1503–21. [PubMed: 15931389]

34. Leung C, Lingbeek M, Shakhova O, Liu J, Tanger E, Saremaslani P, et al. Bmi1 is essential for cerebellar development and is overexpressed in human medulloblastomas. Nature. 2004 Mar 18; 428(6980):337–41. [PubMed: 15029199]

35. Prince ME, Sivanandan R, Kaczorowski A, Wolf GT, Kaplan MJ, Dalerba P, et al. Identification of a subpopulation of cells with cancer stem cell properties in head and neck squamous cell carcinoma. Proc Natl Acad Sci U S A. 2007 Jan 16; 104(3):973–8. [PubMed: 17210912]

36. Chiba T, Miyagi S, Saraya A, Aoki R, Seki A, Morita Y, et al. The polycomb gene product BMI1 contributes to the maintenance of tumor-initiating side population cells in hepatocellular carcinoma. Cancer Res. 2008 Oct 1; 68(19):7742–9. [PubMed: 18829528]

37. Lukacs RU, Memarzadeh S, Wu H, Witte ON. Bmi-1 is a crucial regulator of prostate stem cell self-renewal and malignant transformation. Cell Stem Cell. 2010 Dec 3; 7(6):682–93. [PubMed: 21112563]

38. Yang MH, Hsu DS, Wang HW, Wang HJ, Lan HY, Yang WH, et al. Bmi1 is essential in Twist1-induced epithelial-mesenchymal transition. Nat Cell Biol. 2010 Oct; 12(10):982–92. [PubMed: 20818389]

39. Yang WH, Lan HY, Huang CH, Tai SK, Tzeng CH, Kao SY, et al. RAC1 activation mediates Twist1-induced cancer cell migration. Nat Cell Biol. 2012 Mar 11.

40. Lavial F, Bessonnard S, Ohnishi Y, Tsumura A, Chandrashekran A, Fenwick MA, et al. Bmi1 facilitates primitive endoderm formation by stabilizing Gata6 during early mouse development. Genes Dev. 2012 Jul 1; 26(13):1445–58. [PubMed: 22713603]

41. Liu A, Feng B, Gu W, Cheng X, Tong T, Zhang H, et al. The CD133+ subpopulation of the SW982 human synovial sarcoma cell line exhibits cancer stem-like characteristics. Int J Oncol. 2013 Apr; 42(4):1399–407. [PubMed: 23416969]

42. Zhang Y, Wang Z, Yu J, Shi J, Wang C, Fu W, et al. Cancer stem-like cells contribute to cisplatin resistance and progression in bladder cancer. Cancer Lett. 2012 Sep 1; 322(1):70–7. [PubMed: 22343321]

43. Choijamts B, Jimi S, Kondo T, Naganuma Y, Matsumoto T, Kuroki M, et al. CD133+ cancer stem cell-like cells derived from uterine carcinosarcoma (malignant mixed Mullerian tumor). Stem Cells. 2011 Oct; 29(10):1485–95. [PubMed: 21919130]

44. Niggeweg R, Kocher T, Gentzel M, Buscaino A, Taipale M, Akhtar A, et al. A general precursor ion-like scanning mode on quadrupole-TOF instruments compatible with chromatographic separation. Proteomics. 2006 Jan; 6(1):41–53. [PubMed: 16302280]

45. Steen H, Kuster B, Fernandez M, Pandey A, Mann M. Detection of tyrosine phosphorylated peptides by precursor ion scanning quadrupole TOF mass spectrometry in positive ion mode. Anal Chem. 2001 Apr 1; 73(7):1440–8. [PubMed: 11321292]
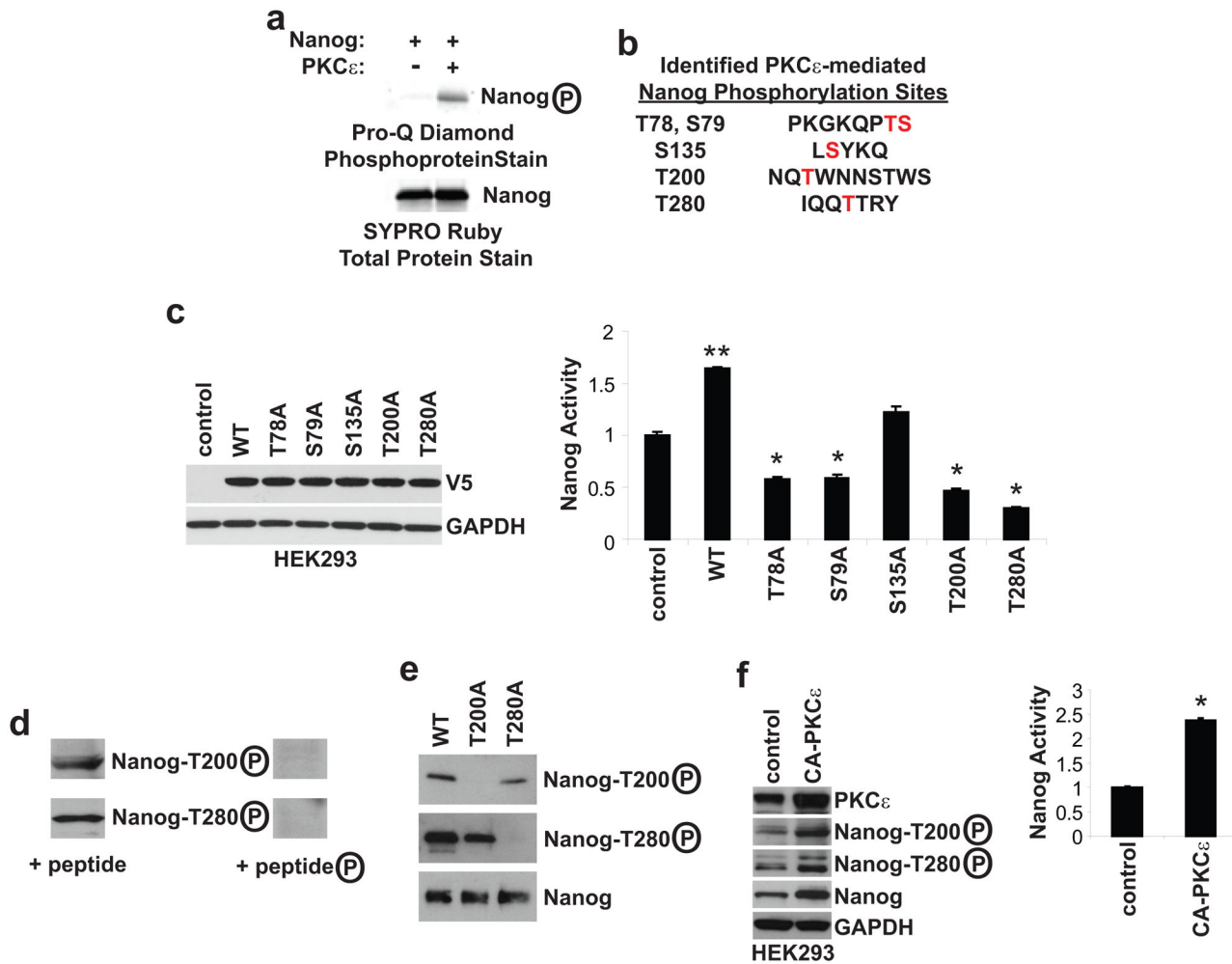
Figure 1. Phosphorylation enhances Nanog transcriptional activity

(a) PKCε phosphorylates Nanog *in vitro*. Recombinant human wildtype Nanog was incubated with or without recombinant human wildtype PKCε in kinase buffer containing PKC activators, phosphatidylserine and diacylglycerol, and ATP for 30 minutes at 25°C. Subsequently, the incubation reaction was terminated, separated by SDS-PAGE, and stained using SYPRO Ruby and Pro-Q Diamond to visualized total protein and phosphorylated protein, respectively. (b) Phosphopeptide mapping of Nanog. Nanog was phosphorylated with PKCε *in vitro* and digested with enzymes to generate peptide fragments. Nanog peptide fragments were analyzed with liquid chromatography-mass spectrometry/mass spectrometry (LC-MS/MS) to identify the phosphorylation sites. (c) Nanog transcriptional activity. HEK293/Nanog-TRE cells were transfected with empty vector (control), V5-tagged wildtype Nanog, V5-tagged T78A mutant Nanog, V5-tagged S79A mutant Nanog, V5-tagged S135A mutant Nanog, V5-tagged T200A mutant Nanog, or V5-tagged T280A mutant Nanog and selected in antibiotics to generate stable polyclonal populations. V5-tagged wildtype/mutant Nanog levels were assessed by immunoblot analysis. Nanog transcriptional activity was measured using a luminometer. Data is presented and mean ± SEM. *$P<0.001$, n=5, control vs. mutant Nanog; **$P<0.001$, n=5, control vs. wildtype

Nanog. (d and e) Validation of phospho-T200 and phospho-T280 Nanog antibodies. (d) Competition with phosphopeptide or nonphosphopeptide. Phospho-T200 antibody were incubated with 10X molar excess of phosphopeptide (PMWSNQ[pT]WNNSTW) or nonphosphopeptide (PMWSNQTWNNSTW). Phospho-T280 antibody were incubated with 10X molar excess of phosphopeptide (LNVIQQ[pT]TRYFST) or nonphosphopeptide (LNVIQQTTRYFST). The antibody:peptide mixtures were incubated overnight at 4°C and subsequently used to detect phosphorylated Nanog using UMSCC74A lysates. (e) Detection of recombinant T200A and T280A mutant Nanog. Recombinant T200A and T280A mutant Nanog were separated by SDS-PAGE and transferred to nitrocellulose membrane. Phosphorylation of Nanog at T200 and T280 was assessed by immunoblot analysis with phospho-T200 and phospho-T280 Nanog antibodies. (f) PKCε phosphorylates Nanog *in vivo*. HEK293 cells were transduced with Cignal Lenti Nanog Reporter and stable polyclonal HEK293/Nanog-TRE cells were generated by selection in puromycin. HEK293/Nanog-TRE cells were transfected with empty vector (control) or constitutive active (A159E) PKCε. PKCε, Nanog, and phospho-T200/T280 levels were assessed by immunoblot analysis. Nanog transcriptional activity was measured using a luminometer. Data is presented and mean ± SEM. *P<0.0001, n=5.
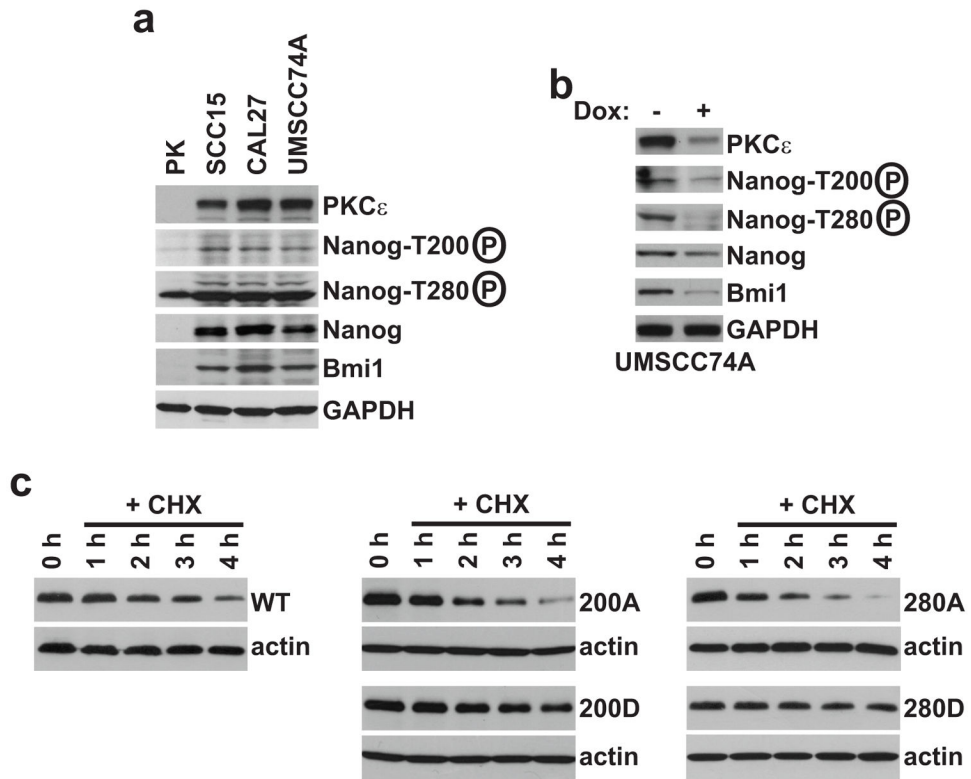
Figure 2. Phosphorylation enhances Nanog protein stability
(a) PKCε, Nanog, phospho-T200/T280 Nanog, and Bmi1 levels in HNSCC cells. Protein levels were assessed using immunoblot analysis. (b) PKCε, Nanog, phospho-T200/T280 Nanog, and Bmi1 levels in PKCε-deficient UMSCC74A cells. UMSCC74A/inducible shRNA-PKCε cells were induced with vehicle or doxycycline for 48 hours. Protein levels were assessed using immunoblot analysis. (c) Nanog protein half-life. Stable polyclonal UMSCC74A/V5-wildtype Nanog, UMSCC74A/V5-T200A, UMSCC74A/V5-T200D, UMSCC74A/V5-T280A, and UMSCC74A/V5-T280D cells were treated with cycloheximide (10 μM) for 1, 2, 3, and 4 hours. Cell lysates were prepared and assessed for V5-tagged Nanog levels using immunoblot analysis. Representative blots are shown from 3 independent experiments.
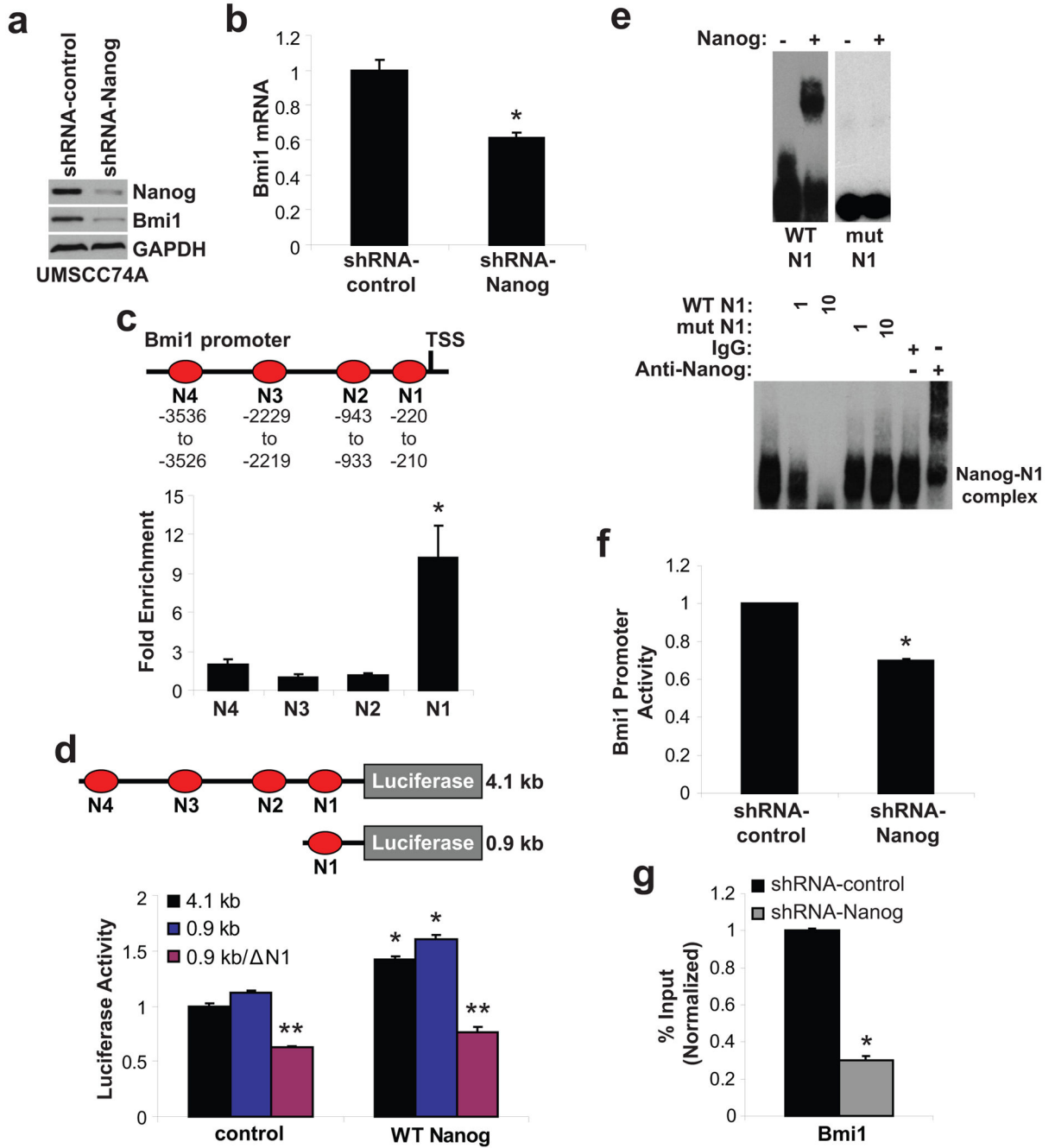
a

UMSCC74A

Nanog
Bmi1
GAPDH

b

c

Bmi1 promoter   TSS

N4   N3   N2   N1
-3536   -2229   -943   -220
to   to   to   to
-3526   -2219   -933   -210

d

Luciferase 4.1 kb
N4 N3 N2 N1

Luciferase 0.9 kb
N1

e

Nanog-N1 complex

f

g

Figure 3. Nanog regulates Bmi1 through promoter occupancy

(a) Genetic ablation of Nanog reduces Bmi1 levels. Cell lysates were prepared and assessed for Nanog and Bmi1 levels by immunoblot analysis. (b) Bmi1 mRNA expression. Total mRNA was prepared using Trizol and qPCR analysis was performed using validated Bmi1 TaqMan primers. Data is presented as mean $\pm$ SEM. *P<0.01, n=3. (c) Nanog occupies the Bmi1 promoter. Bmi1 promoter analysis identified four putative Nanog binding sites. ChIP was performed on UMSCC74A cells using an anti-Nanog or anti-IgG antibody. Immunoprecipitated complexes were detected with real-time qPCR using primers specific to

the N1, N2, N3, and N4 sites in the Bmi1 promoter. Fold enrichment was normalized to anti-IgG and presented as mean ± SEM. *P<0.001, n=4. (d) Bmi1 promoter activity. HEK293/empty and HEK293/wildtype Nanog cells were co-transfected with the 4.1 kb, 0.9 kb (contains N1 site only), or 0.9 kb/ N1 (deletion of N1 site) Bmi1 promoter-Renilla luciferase and the CMV-Firefly luciferase plasmids. Bmi1 promoter activity was normalized with CMV-Firefly luciferase to control for transfection efficiency and presented as mean ± SEM. *P<0.005, n=3, empty vs. WT Nanog using 4.1 kb or 0.9 kb Bmi1 promoter; **P<0.005, n=3, 4.1 kb or 0.9 kb Bmi1 promoter vs. 0.9 kb/ N1 Bmi1 promoter in control or WT Nanog cells. (e) Electrophoretic mobility shift assay. Recombinant human wildtype Nanog was assessed for binding to the wildtype or mutant N1 oligonucleotides using EMSA (top panel). Competition EMSA was performed by incubating nuclear extracts from UMSCC74A cells with excess (1X or 10X molar) unlabeled wildtype or mutant N1 oligonucleotides in the presence of labeled wildtype N1 oligonucleotide (bottom panel, left lanes). Supershift assay using an anti-Nanog antibody was performed to confirm Nanog binding to the N1 site (bottom panel, right lanes). (f) Bmi1 promoter activity. Bmi1 promoter (0.9 kb) activity was measured using a luminometer. Data is normalized to shRNA-control and presented as mean ± SEM. *P<0.001, n=5. (g) Bmi1 promoter occupancy. ChIP was performed on UMSCC74A/shRNA-control and UMSCC74A/shRNA-Nanog cells using an anti-Nanog or anti-IgG antibody. Immunoprecipitated complexes were detected with real-time qPCR using a primer set specific to the N1 site in the Bmi1 promoter. ChIP with an anti-IgG antibody was used as the negative control. % input was normalized to anti-IgG for shRNA-control and shRNA-Nanog. Data is normalized to shRNA-control and presented as mean ± SEM. *P<0.0001, n=4.
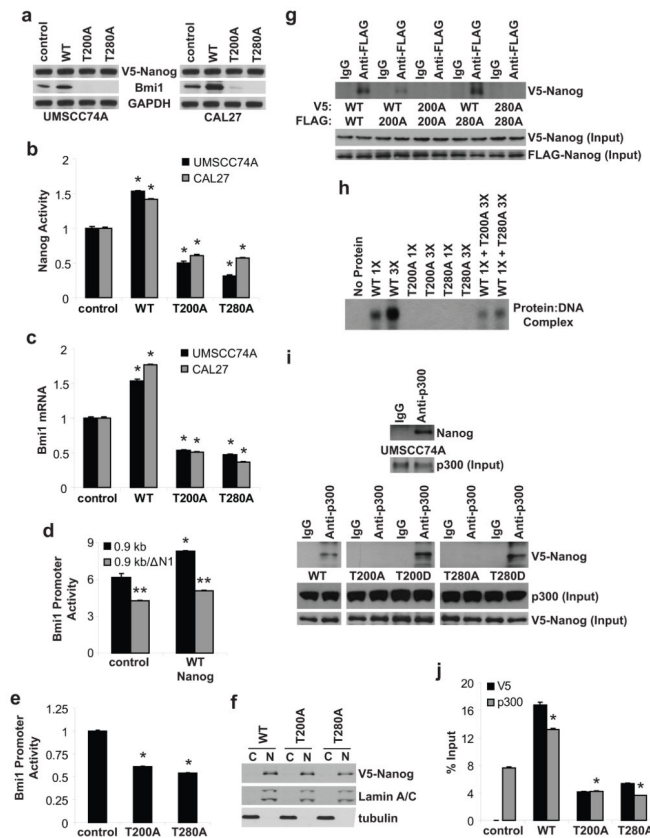
Figure 4. Phosphorylation of Nanog modulates homodimerization and Bmi1 promoter occupancy and transactivation

(a) T200A and T280A mutant Nanog reduce Bmi1 levels in HNSCC cells. UMSCC74A cells were transfected with empty vector (control), wildtype Nanog (WT), T200A mutant Nanog, or T280A mutant Nanog and selected in antibiotics to generate stable polyclonal populations. V5-tagged Nanog and Bmi1 levels were assessed by immunoblot analysis. (b) Nanog transcriptional activity. Nanog transcriptional activity was measured using a luminometer. Data is presented and mean ± SEM. *P<0.0001, n=5. (c) Bmi1 mRNA expression. Total mRNA was prepared using Trizol and qPCR analysis was performed using validated Bmi1 TaqMan primers. Data is presented as mean ± SEM. *P<0.01, n=3. (d) Bmi1 promoter activity. Bmi1 promoter (0.9 kb or 0.9 kb/ N1) activity was measured using a luminometer. Relative Bmi1 promoter-luciferase activity is shown and presented as mean ± SEM. *P<0.001, n=3, control vs. WT Nanog using the 0.9 kb Bmi1 promoter; **P<0.001, n=3, 0.9 kb Bmi1 promoter vs. 0.9 kb/ N1 Bmi1 promoter. (e) Bmi1 promoter activity. Bmi1 promoter (0.9 kb) activity was measured using a luminometer. Data is normalized to control and presented as mean ± SEM. *P<0.001, n=5, control vs. T200A or T280A. (f) Nanog localization. Cytosolic (C) and nuclear (N) proteins were isolated from V5-tagged wildtype, T200A, and T280A Nanog UMSCC74A cells. V5-Nanog was detected by immunoblot analysis. (g) Nanog homodimerization. HEK293 cells were co-transfected with V5-tagged wildtype/mutant Nanog and FLAG-tagged wildtype/mutant Nanog. Cell lysates were immunoprecipitated with an anti-FLAG antibody and immunoblotted with an anti-V5 antibody. Input controls for V5-tagged wildtype/mutant Nanog and FLAG-tagged wildtype/

mutant Nanog are presented. (h) DNA binding. Recombinant FLAG-tagged wildtype/mutant Nanog was assessed for binding to the Site1 response element in the Bmi1 promoter using EMSA. (i) p300 association. UMSCC74A cells were untransfected or transfected with V5-tagged wildtype Nanog or mutant Nanog and stable polyclonal populations were selected. Cell lysates from UMSCC74A (upper panel) or UMSCC74A/control, UMSCC74A/wildtype Nanog, or UMSCC74A/mutant Nanog (lower panel) were immunoprecipitated with an anti-p300 antibody and immunoblotted with an anti-Nanog or anti-V5 antibody. Input controls for p300 and V5-tagged Nanog are presented. (j) Bmi1 promoter occupancy. Chromatin immunoprecipitation was performed using an anti-p300 or anti-V5 antibody. Immunoprecipitated complexes were detected with real-time PCR using a primer set specific to the N1 site in the Bmi1 promoter. Chromatin immunoprecipitation with an anti-IgG antibody was used as the negative control. Data (% input) is normalized to IgG and presented as mean ± SEM. *P<0.0001, n=4.
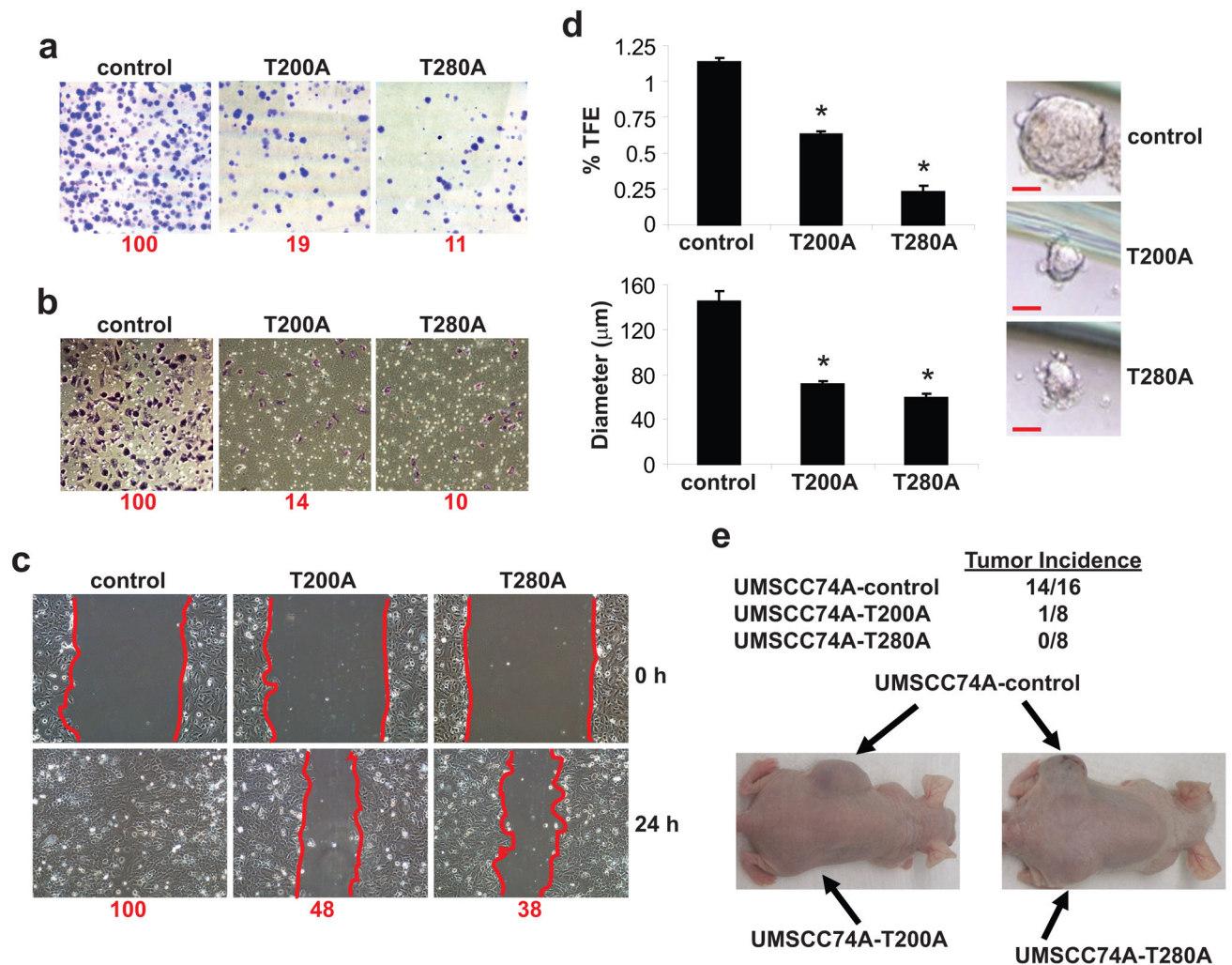
Figure 5. Pleiotropic anti-cancer effects of phosphorylation-insensitive Nanog mutants
(a) Clonogenic survival. Colonies were stained with crystal violet. *P<0.01, n=3. (b) Cell invasion. Cell invasion was assessed using the Modified Boyden chamber invasion assay with Matrigel basement membrane. *P<0.01, n=3. (c) Cell migration. Cell migration was assessed using the wound healing assay. *P<0.01, n=3. (d) Cancer initiating cell number and size. Cells were harvested and seeded on low-attachment plates in a defined, serum-free culture medium at a density of 300 cells/well. Tumorspheres were allowed to grow for 7 days. Tumorsphere formation efficiency was calculated as the number of tumorspheres (50 μm in diameter) formed divided by the original number of cells seeded. Data is presented as mean ± SEM. *P<0.01, n=6. A representative tumorsphere is shown for each cell line. Scale bar, 50 μm. (e) *In vivo* tumor incidence. UMSCC74A-control, UMSCC74A-T200A, and UMSCC74A-T280A cells (1×10^6 cells) were suspended in DMEM (50:50 Matrigel) and implanted subcutaneously in the flanks of athymic nude mice. Tumor incidence was monitored for 68 days post-implantation.
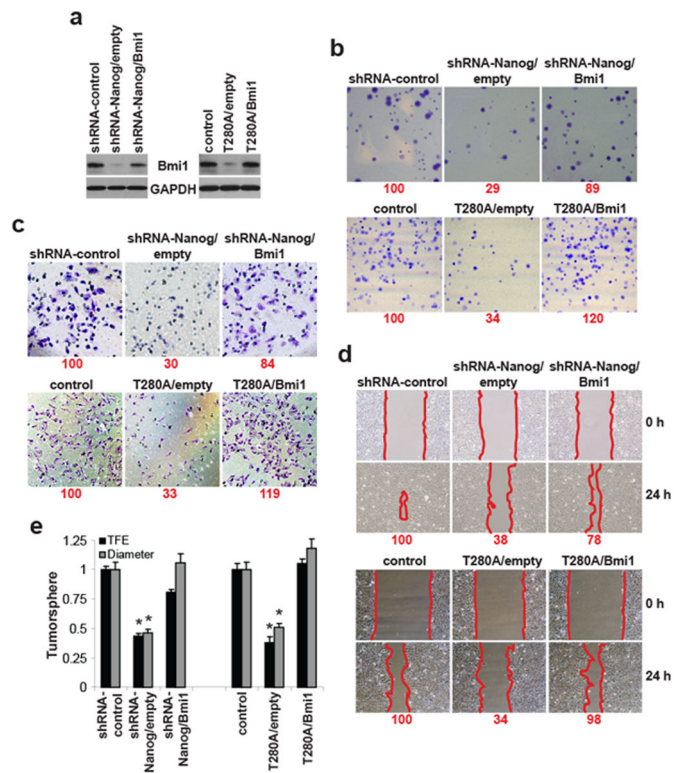
Figure 6. Bmi1 is essential for Nanog-induced tumorigenesis
(a) Bmi1 rescue in Nanog-deficient and T280A mutant Nanog cells. Cell lysates were prepared and assessed for Bmi1 levels by immunoblot analysis. (b) Clonogenic survival. Colonies were stained with crystal violet and counted. * *P*<0.01, n=3. (c) Cell invasion. Cell invasion was assessed using the Modified Boyden chamber invasion assay with Matrigel basement membrane. *P*<0.01, n=3. (d) Cell migration. Cell migration was assessed using the wound healing assay. *P*<0.01, n=3. (e) Cancer initiating cell number and size. Cells were harvested and seeded on low-attachment plates in a defined, serum-free culture medium at a density of 300 cells/well. Tumorspheres were allowed to grow for 7 days. Tumorsphere formation efficiency was calculated as the number of tumorspheres (50 μm in diameter) formed divided by the original number of cells seeded. Data is presented as mean ± SEM. *P*<0.01, n=6.
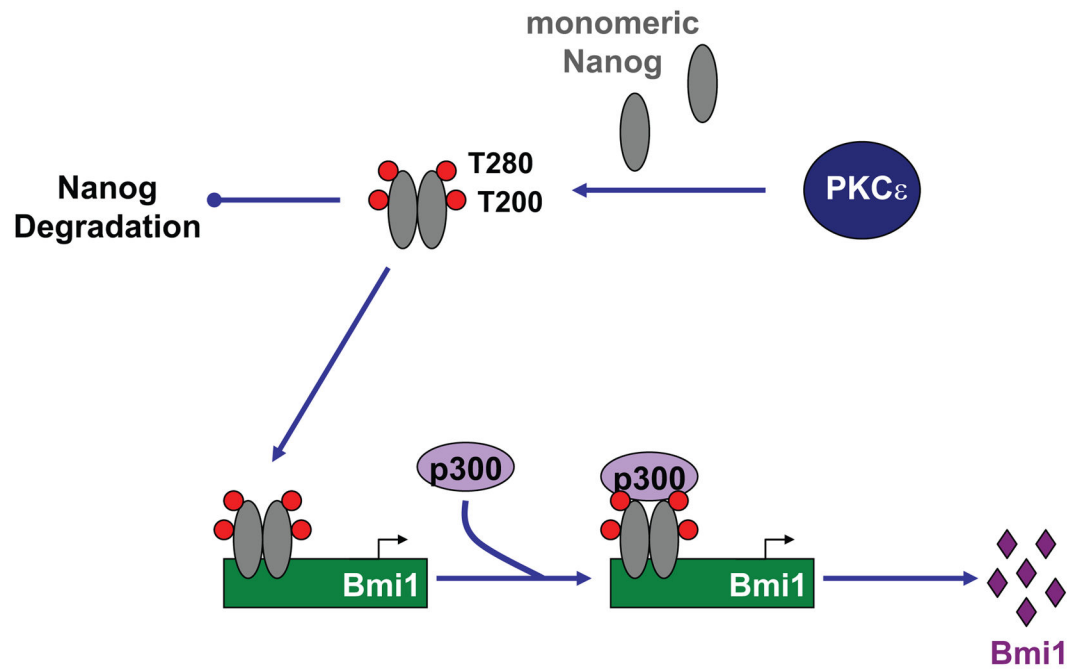
Figure 7. A proposed model of the PKCε-Nanog-Bmi1 signaling axis in tumorigenesis
PKCε phosphorylates Nanog at T200 and T280 to enhance Nanog stability, homodimerization and Bmi1 promoter occupancy. Subsequently, the p300 co-activator is recruited to facilitate Bmi1 promoter transactivation.